

Glassy dielectric anomaly and negative magneto-capacitance effect in electron-doped $\text{Ca}_{1-x}\text{Sr}_x\text{Mn}_{0.85}\text{Sb}_{0.15}\text{O}_3$

Haruka Taniguchi,^{1, a)} Hidenori Takahashi,¹ Akihiro Terui,¹ Kensuke Sadamitsu,¹ Yuka Sato,¹ Michihiro Ito,¹ Katsuhiko Nonaka,¹ Satoru Kobayashi,¹ Michiaki Matsukawa,¹ Ramanathan Suryanarayanan,² Nae Sasaki,³ Shunpei Yamaguchi,³ and Takao Watanabe³

¹⁾*Iwate University, Morioka 020-8551, Japan*

²⁾*Université Paris-Sud, 91405 Orsay, France (Retired)*

³⁾*Hirosaki University, Hirosaki, 036-8561, Japan*

(Dated: 28 February 2022)

Manganites exhibit various types of electronic phenomena, and these electronic characteristics can be controlled by carrier doping. Herein, we report the dielectric and magnetic properties of electron-doped manganite $\text{Ca}_{1-x}\text{Sr}_x\text{Mn}_{0.85}\text{Sb}_{0.15}\text{O}_3$ ($x = 0, 0.1, 0.2$, and 0.3). The temperature dependence of the real part of the dielectric constant exhibits a broad and large peak just below the kink temperature of magnetization and a sharp decrease at lower temperatures, accompanied by an anomaly of the imaginary part. Furthermore, isovalent Sr substitution enhances the temperature of the dielectric peak by more than 50 K. Interestingly, the dielectric peak exhibits a negative magnetic-field effect. For all measured samples, the low-temperature variation of the dielectric constant can be qualitatively explained based on the Maxwell-Wagner (MW) model that describes a system composed of grain boundaries and semiconducting grains. However, the observed peak and its negative magneto-capacitance effect at high temperatures cannot be reproduced by a combination of the MW model and magnetoresistance effect. The dielectric peak strongly indicates polaronic relaxation in the present system. These results suggest that polarons form clusters with a dipole ordering and magneto-electric coupling, which might be consistently understood by the charge-ordering scenario.

PACS numbers: 77.22.-d, 75.85.+t, 75.25.Dk

I. INTRODUCTION

Manganites exhibit various electronic phenomena such as charge-orbital ordering, colos-

^{a)}tanig@iwate-u.ac.jp

sal magnetoresistance, and phase separation because of the competition or cooperation between electron–electron interactions (for example, between ferromagnetic double exchange interaction and antiferromagnetic (AFM) superexchange interaction)¹. Carrier doping is a powerful tool to control the electronic state of manganites. For example, electron-doped systems $\text{CaMn}_{1-x}\text{Mo}_x\text{O}_3$ and $\text{Ca}_{1-x}\text{Ce}_x\text{MnO}_3$ change the ground state from a G-type AFM ordering to a charge/orbital-ordered C-type AFM ordering^{2–5}. In another electron-doped system $\text{Ca}_{1-x}\text{La}_x\text{MnO}_3$, dielectric properties were reported^{6,7}. With respect to hole-doped systems, $\text{Pr}_{1-x}\text{Ca}_x\text{MnO}_3$ and $\text{Y}_{1-x}\text{Ca}_x\text{MnO}_3$ exhibit an interesting dielectric anomaly, which is sensitive to a magnetic field and is induced around the charge-ordering (CO) temperature^{8–12}.

With the aim to identify new phenomena in manganites, we investigated an electron-doped system $\text{CaMn}_{1-y}\text{Sb}_y\text{O}_3$ for $y \leq 0.1$ ^{13–16}. X-ray photoelectron spectroscopy proved that the valency of Sb is 5+¹⁵. Thus, the substitution of Sb^{5+} ions for Mn^{4+} sites causes one-electron doping with the chemical formula $\text{Ca}^{2+}\text{Mn}_{1-2y}^{4+}\text{Mn}_y^{3+}\text{Sb}_y^{5+}\text{O}_3^{2-}$ accompanied by a monotonic increase of unit-cell volume as a function of y . From the magnetization and AC-susceptibility measurements, a canted AFM ordering is expected below the Neel temperature of 100 K^{13–16}. Interestingly, we revealed magnetization reversal after field-cooling for $0.02 \leq$

$y \leq 0.08$ ^{13,14} probably because the local lattice distortion of MnO_6 octahedra induced by the Sb substitution changed the orbital state of the e_g electron of Mn^{3+} and reversed the local easy axis of magnetization. For $y = 0.05$, the physical and chemical pressure effects were also reported^{15,16}.

Just recently, we started studying the dielectric properties of $\text{CaMn}_{0.85}\text{Sb}_{0.15}\text{O}_3$ ¹⁷ because manganites provide interesting dielectric materials such as magnetoelectrics and relaxors. Interestingly, we found a broad and large peak in the temperature dependence of the dielectric constant, which exhibited a negative magnetic-field effect. Considering the broadness and large value of the peak, $\text{CaMn}_{0.85}\text{Sb}_{0.15}\text{O}_3$ might be a dielectric glass. The magnetic-field-sensitive dielectric constant suggests that $\text{CaMn}_{0.85}\text{Sb}_{0.15}\text{O}_3$ is a new magnetoelectric material. Four cases are known to be the origin of magnetoelectrics: magnetic exchange striction^{18,19}, inverse Dzyaloshinskii-Moriya interaction^{20,21}, d - p hybridization²², and CO^{23–30}. For $\text{CaMn}_{0.85}\text{Sb}_{0.15}\text{O}_3$, where both Mn^{3+} and Mn^{4+} ions exist, the formation of CO is expected suggesting a correlation between the CO and the observed magnetocapacitance effect. CO-originated magnetoelectrics can be realized under these two conditions: (1) the condition for macroscopic electric polarization—where the pattern of CO does not have an inversion symmetry; (2) the condition

for magneto-electric coupling—where the CO accompanies a magnetic ordering with a one-to-one correspondence between the pattern of the CO and that of the magnetic ordering. In such a case, the direction of the electric polarization is also controlled by a magnetic field through a change in the pattern of magnetic ordering.

In this study, to clarify the origin of the magneto-capacitance effect of $\text{CaMn}_{0.85}\text{Sb}_{0.15}\text{O}_3$, we compared the dielectric, conducting, and magnetic properties in detail. Moreover, to determine whether $\text{CaMn}_{0.85}\text{Sb}_{0.15}\text{O}_3$ is a dielectric glass, we investigated the frequency dependence of the dielectric constant of $\text{Ca}_{1-x}^{2+}\text{Sr}_x^{2+}\text{Mn}_{0.85}\text{Sb}_{0.15}\text{O}_3$ ($x = 0, 0.1, 0.2, 0.3$).

II. EXPERIMENTAL

Polycrystalline samples of $\text{Ca}_{1-x}\text{Sr}_x\text{Mn}_{0.85}\text{Sb}_{0.15}\text{O}_3$ ($x = 0, 0.1, 0.2$, and 0.3) were prepared by a solid-state reaction method. The stoichiometric mixtures of CaCO_3 , SrCO_3 , Mn_3O_4 , and Sb_2O_3 powders were calcined in air at 1000°C for 48 h. The products were ground and pressed into disk-like pellets. The pellets were sintered at 1350°C for 48 h. Single crystalline samples were grown by the floating zone method in Ar atmosphere using the polycrystal of $\text{CaMn}_{0.85}\text{Sb}_{0.15}\text{O}_3$. We performed the quantitative composition analysis using the electron probe micro analyzer

(JXA-8500F, JEOL). The compositions of the obtained polycrystalline samples are the same as those of the mixed samples, whereas that of single crystalline samples is found to be $\text{CaMn}_{0.88}\text{Sb}_{0.12}\text{O}_3$. We also performed X-ray diffraction measurements at approximately 290 K using an Ultima IV diffractometer (Rigaku) with $\text{Cu K}\alpha$ radiation.

We measured the dielectric constant under several frequencies and DC magnetic fields using the parallel mode of an LCR meter (Agilent, E4980A). Samples were cut into a parallel plate with an area of $3.2 \times 6.0 \text{ mm}^2$ and a thickness of 0.7 mm, and Au wires for electric lead were connected by Ag paint (Dupont, 4929N). To reduce the contact resistance, sample surfaces were polished to be flat using $9 \mu\text{m}$ diamond slurry, and Ag paint was heated at 110°C for 30 min. We performed measurements with an AC electric field of 1 V/mm and 10 - 500 kHz under 0 - 5 T (field cooling), obtained the capacitance C and dielectric loss $\tan \delta$, and estimated the real and imaginary part of the relative dielectric constant ϵ'_r and ϵ''_r . To investigate the magnetic properties as well, we measured magnetization using a commercial SQUID magnetometer (Quantum Design, MPMS) under 10 mT after field cooling. DC resistivity and specific heat were measured using the Physical Property Measurement System (Quantum Design).

III. RESULTS

Figure 1 (a) presents the X-ray diffraction spectrum of $\text{Ca}_{1-x}\text{Sr}_x\text{Mn}_{0.85}\text{Sb}_{0.15}\text{O}_3$ ($x = 0, 0.1, 0.2$, and 0.3). Based on the previous study on orthorhombic $\text{CaMn}_{0.9}\text{Sb}_{0.1}\text{O}_3$ and monoclinic $\text{CaMn}_{0.8}\text{Sb}_{0.2}\text{O}_3$ ³¹, (101) and (020) peaks are expected at approximately 23.5° in both the orthorhombic and monoclinic cases, and (10-1) peak appears at a slightly lower angle in the monoclinic case. As shown in Fig. 1 (b), all the samples exhibited a peak at approximately 23.5° and 23.8° , which suggests the (101) and (020) reflection, respectively. In addition, another peak appeared at approximately 23.1° for $x \geq 0.1$, although the peak for $x = 0.1$ was as small as background fluctuation. Therefore, we consider that the $x = 0$ sample had a $Pnma$ orthorhombic structure, whereas the $x \geq 0.2$ samples were described by a $P2_1/m$ monoclinic structure. The sample of $x = 0.1$ might be located at the boundary between the orthorhombic and monoclinic phases. These results are similar to the structural variation in other partially substituted manganites $\text{CaMn}_{1-x}\text{Mo}_x\text{O}_3$ and $\text{Ca}_{1-x}\text{Ce}_x\text{MnO}_3$ ³⁻⁵. A stronger intensity at approximately 23.8° for $x = 0.1$, compared with intensity of the other compositions, suggests that grinding was imperfect for the powder sample of $x = 0.1$, and the distribution of the relative angle between the X-ray incidence and the crystallographic axis of

the sample was not uniform. Consistently, the (040) peak at approximately 47.9° was also relatively high at $x = 0.1$, and similarly for the (020) peak at approximately 23.8° . The obtained lattice parameters and unit cell volume are plotted in Fig. 1 (c). The values of a , b , and c exhibit a monotonic increase with Sr substitution. This substitution effect is consistent with the fact that the ion radius of Sr^{2+} is larger than that of Ca^{2+} .

As shown in Fig. 2 (a), the value of the electrical resistivity ρ of $\text{Ca}_{1-x}\text{Sr}_x\text{Mn}_{0.85}\text{Sb}_{0.15}\text{O}_3$ is smaller than that of typical insulators by several orders of magnitude. We found that a value of $\rho(T)$ above 190 K can be described by the small polaron hopping model $\rho = \rho_0 T \exp(E_{a,\rho}/k_B T)$. The values of the activation energy $E_{a,\rho}$ estimated from the fitting shown in Fig. 2 (b) are listed in Table I. As shown in the inset of Fig. 2 (b), the temperature dependence of the local activation energy $E_{\text{local}} = d(\ln \rho)/d(1/T)$ exhibits a small jump-like anomaly. The fact that both Mn^{3+} and Mn^{4+} ions exist in $\text{CaMn}_{0.85}\text{Sb}_{0.15}\text{O}_3$ makes CO a reasonable candidate for the transport anomaly. Because the anomaly is small, CO is expected to be realized only in several fractions in the sample not in the whole sample. This short-range cluster scenario is supported also by the fact that substituted Sb ions act as impurities in the Mn lattice as well as dope electrons and suppress the Mn-Mn interaction. The anomaly temperature T_ρ is

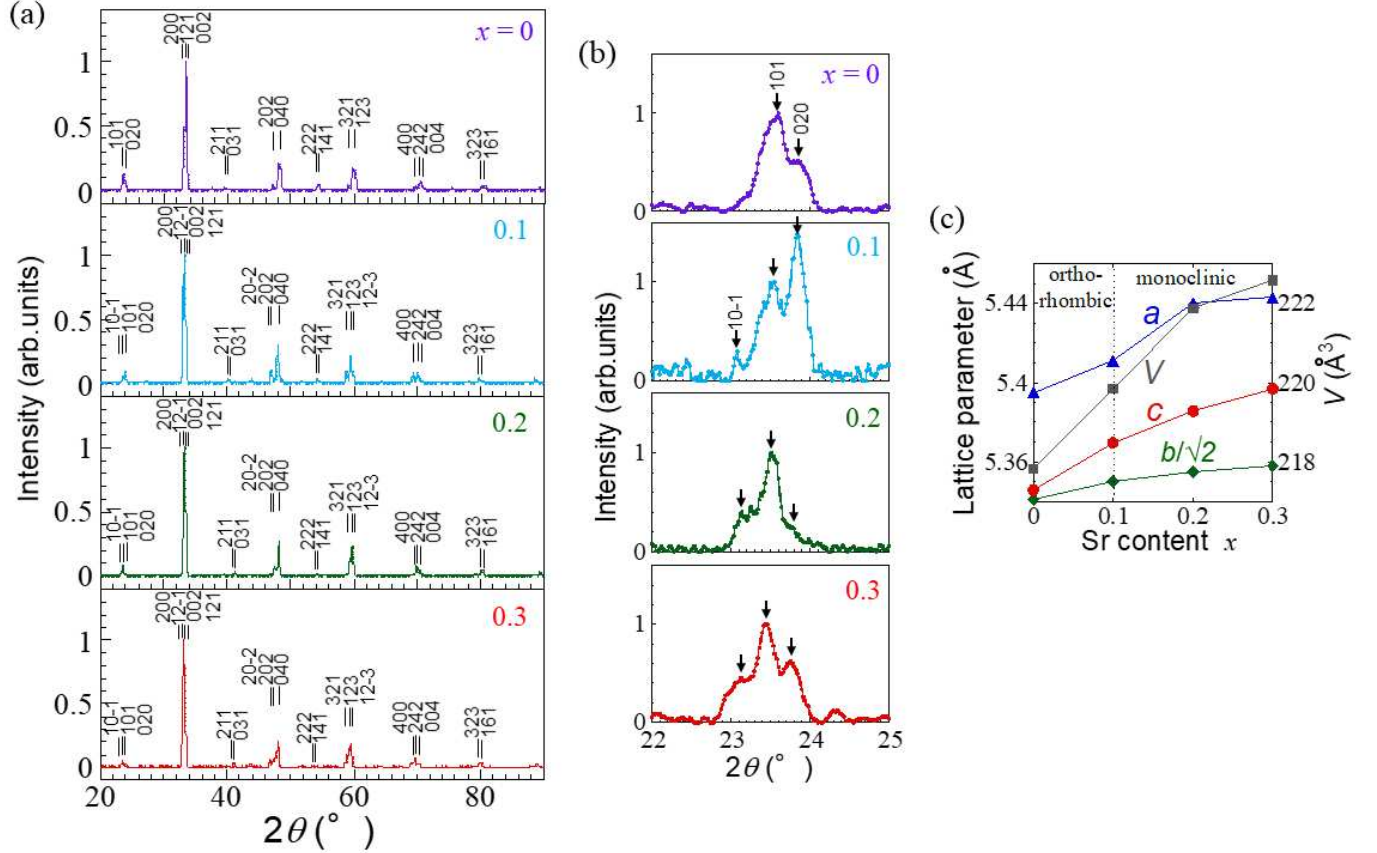


FIG. 1. (a) X-ray diffraction spectrum of polycrystalline $\text{Ca}_{1-x}\text{Sr}_x\text{Mn}_{0.85}\text{Sb}_{0.15}\text{O}_3$ ($x = 0, 0.1, 0.2$ and 0.3) normalized for the intensity of the highest peak to be 1. (b) Enlarged view of $(10-1)$, (101) , and (020) peaks. The intensity of the (101) peak is normalized to be 1. (c) Lattice parameters and unit cell volume of $\text{Ca}_{1-x}\text{Sr}_x\text{Mn}_{0.85}\text{Sb}_{0.15}\text{O}_3$.

listed in Table I. As shown in Fig. 2 (c), the magnetoresistance of $\text{CaMn}_{0.85}\text{Sb}_{0.15}\text{O}_3$ at 1 T appears to be within the error margin.

As shown in Fig. 2 (d), the temperature dependence of magnetization M exhibits a kink at a higher temperature and a remarkable increase at lower temperatures. The kink suggests a magnetic order accompanied by a CO because the kink temperature $T_{M\text{-kink}}$ is near T_p in $\text{Ca}_{1-x}\text{Sr}_x\text{Mn}_{0.85}\text{Sb}_{0.15}\text{O}_3$.

As shown in Fig. 2 (e), the specific heat of $\text{CaMn}_{0.85}\text{Sb}_{0.15}\text{O}_3$ exhibits an anomaly near $T_{M\text{-kink}}$, suggesting phase transition. By analogy with $\text{Ca}_{1-x}\text{Ce}_x\text{MnO}_3$ ⁴, in which CO is proved by a neutron diffraction and a similar magnetic kink is observed at the CO temperature², C-type AFM ordering is expected to be formed below $T_{M\text{-kink}}$ in $\text{Ca}_{1-x}\text{Sr}_x\text{Mn}_{0.85}\text{Sb}_{0.15}\text{O}_3$. The sharp increase in the magnetization below $T_{M\text{-inc}}$ can be under-

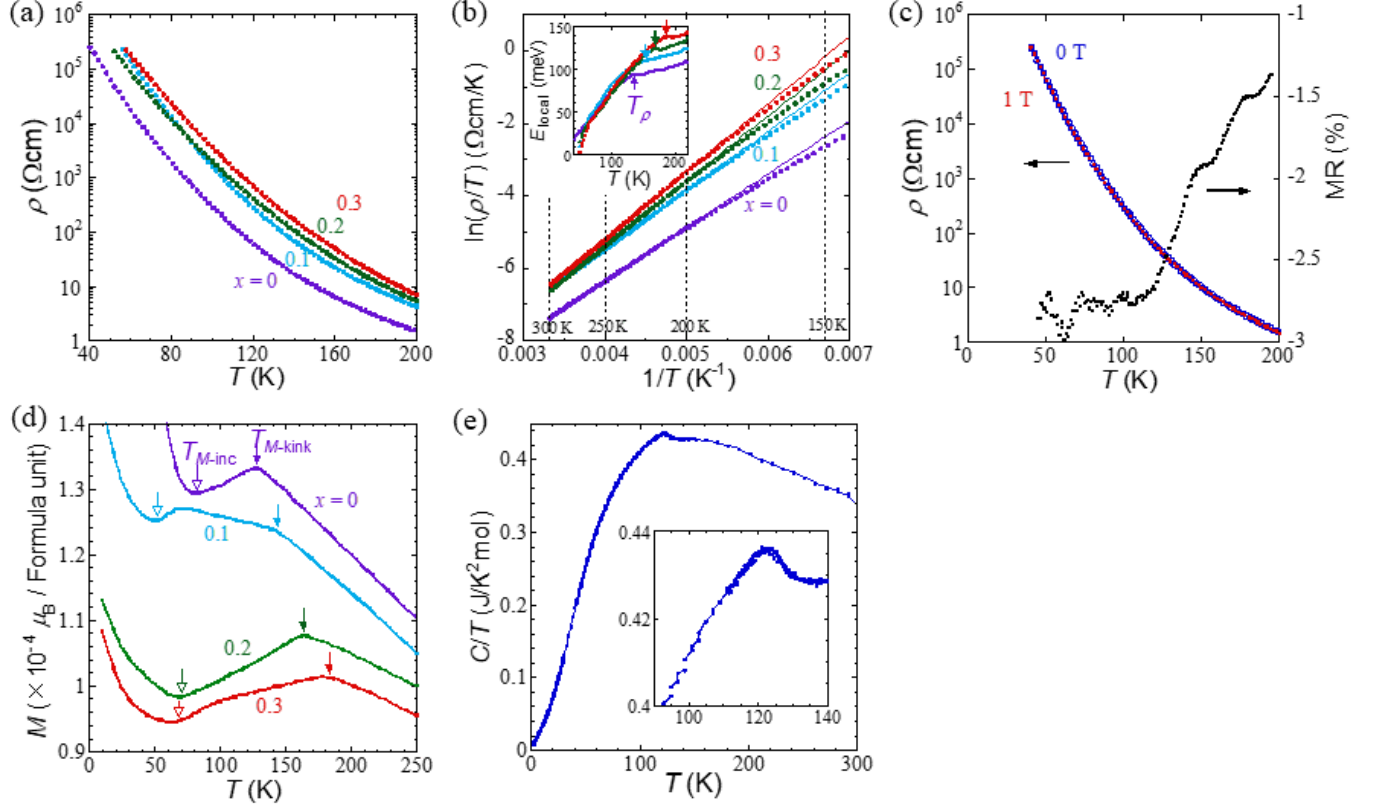


FIG. 2. (a) Temperature dependence of the DC resistivity of polycrystalline $\text{Ca}_{1-x}\text{Sr}_x\text{Mn}_{0.85}\text{Sb}_{0.15}\text{O}_3$ ($x = 0, 0.1, 0.2$ and 0.3). (b) $\ln(\rho/T)$ as a function of $1/T$. The solid lines are the fitting results according to the small polaron hopping model. The inset presents the local activation energy $E_{\text{local}} = d(\ln\rho)/d(1/T)$. Arrows designate a small jump-like anomaly that might suggest the formation of short-range CO clusters. (c) Comparison of the resistivity between 0 T and 1 T for $\text{CaMn}_{0.85}\text{Sb}_{0.15}\text{O}_3$. (d) Temperature dependence of the magnetization measured under 10 mT after field cooling. Filled and open arrows indicate the positions of the kink and the onset of the remarkable increase, respectively. (e) Temperature dependence of the specific heat of polycrystalline $\text{CaMn}_{0.85}\text{Sb}_{0.15}\text{O}_3$. The inset is an enlarged view near the anomaly.

stood as the growth of the canted component of AFM ordering.

In Fig. 3, we show the temperature dependence of the relative dielectric constant of $\text{Ca}_{1-x}\text{Sr}_x\text{Mn}_{0.85}\text{Sb}_{0.15}\text{O}_3$ ($x = 0, 0.1, 0.2$ and 0.3) for several frequencies (10, 50, 100 and 500 kHz). Interestingly, the real part ϵ'_r of each

sample exhibits a common broad peak at an intermediate temperature and then sharply decreases at low temperatures of approximately 50 K. Notably, the temperature of the peak in $\epsilon'_r(T)$ is near the temperatures of the anomaly in $E_{\text{local}}(T)$ and the kink in $M(T)$. In the imaginary part ϵ''_r , a shoulder structure ap-

TABLE I. Characteristic values in the fundamental properties of $\text{Ca}_{1-x}\text{Sr}_x\text{Mn}_{0.85}\text{Sb}_{0.15}\text{O}_3$ ($x = 0, 0.1, 0.2$ and 0.3). $\rho_{100\text{K}}$ and $\rho_{200\text{K}}$ represent the DC resistivities at 100 K and 200 K, respectively. The activation energies $E_{a,p}$ are estimated from the high-temperature resistivity data using a small polaron hopping model. T_p denotes the temperature of the small jump-like anomaly in the local activation energy $E_{\text{local}}(T)$. $T_{M\text{-kink}}$ denotes the kink temperature of magnetization $M(T)$.

x	tolerance factor	$\rho_{100\text{K}}$	$\rho_{200\text{K}}$	$E_{a,p}$	T_p	$T_{M\text{-kink}}$
		(Ωcm)	(Ωcm)	(meV)	(K)	(K)
0.0	0.9896	295.8	1.521	127	137	127
0.1	0.9933	1640	4.262	140	155	143
0.2	0.9969	2027	5.430	155	169	163
0.3	1.000	3622	7.041	161	189	178

appears at approximately 50 K. For understanding $\epsilon_r''(T)$, we should note that conductive charges as well as capacitive charges contribute to ϵ_r'' . Because of the small-polaron-hopping-type temperature dependence and the comparably low value of resistivity, the dielectric loss of $\text{CaMn}_{0.85}\text{Sb}_{0.15}\text{O}_3$ is expected to exhibit an extremely large value at higher temperatures and is expected to be remarkably suppressed on cooling. Comparably large ϵ_r'' was observed in a similar low resistivity system $\text{Pr}_{1-x}\text{Ca}_x\text{MnO}_3$ ³³, in which $\epsilon_r'(T)$ exhibited a broad peak around the CO temperature and the peak was sensitive to a magnetic field. Focusing on the frequency dependence, these three anomalies, the peak, the sharp decrease of $\epsilon_r'(T)$, and the shoulder of $\epsilon_r''(T)$, shift to higher temperatures with increasing frequency. The value of ϵ_r' near the peak

tends to be suppressed in the high frequency region.

Figure 4 presents the effect of magnetic field on the dielectric properties of $\text{Ca}_{1-x}\text{Sr}_x\text{Mn}_{0.85}\text{Sb}_{0.15}\text{O}_3$ ($x = 0, 0.1, 0.2$, and 0.3). We found a remarkable negative magneto-capacitance effect on the real part: the peak of $\epsilon_r'(T)$ was shifted by the magnetic field. The peak height was suppressed in all samples, and the peak temperature was enhanced for $x \geq 0.2$. The magnitude of the magneto-capacitance effect $(\epsilon_r'(1\text{ T}) - \epsilon_r'(0\text{ T})) / \epsilon_r'(0\text{ T})$ at the peak temperature of 0 T was -14.4%, -23.0%, -17.1%, and -22.3% for $x = 0, 0.1, 0.2$, and 0.3 , respectively. The changes in the imaginary part seem small.

We estimate the characteristic temperatures of the three dielectric anomalies, one conduc-

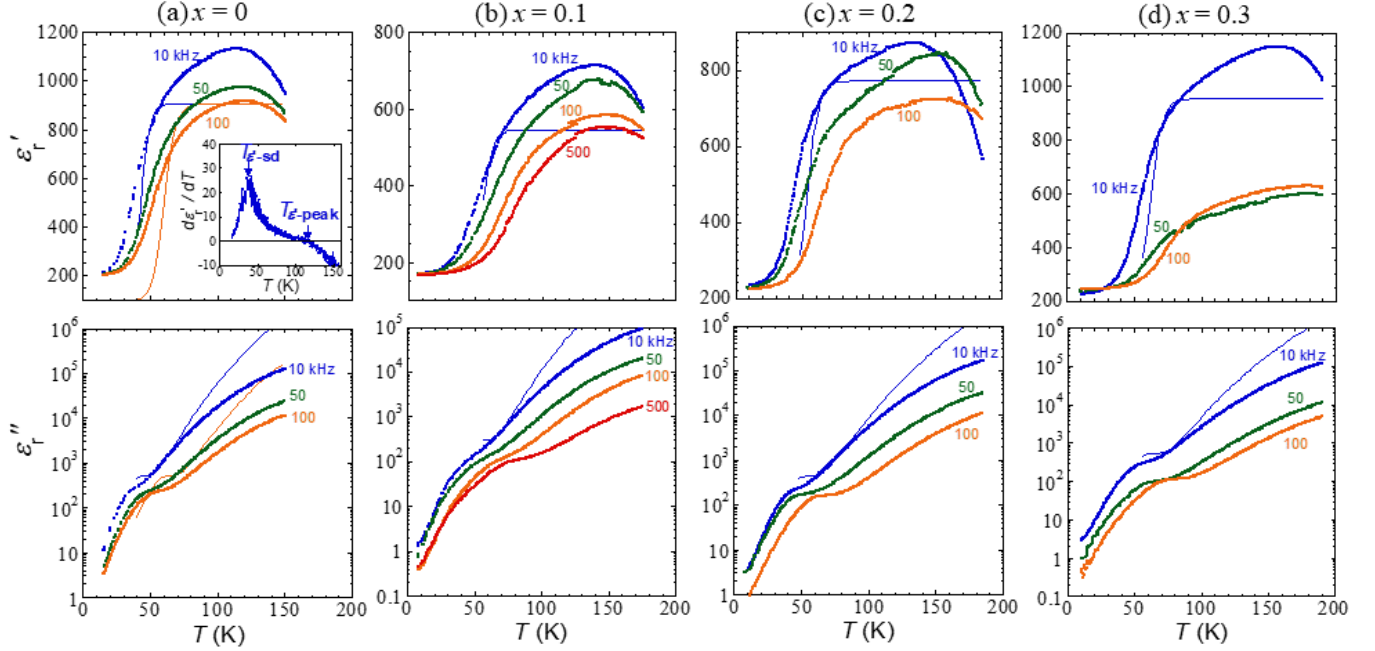


FIG. 3. Temperature dependence of the relative dielectric constant of polycrystalline $\text{Ca}_{1-x}\text{Sr}_x\text{Mn}_{0.85}\text{Sb}_{0.15}\text{O}_3$ under several frequencies. (0 T, AC electric field of 1 V/mm) (a) $x = 0$, (b) $x = 0.1$, (c) $x = 0.2$, and (d) $x = 0.3$. Upper and lower panels represent the real part ϵ'_r and the imaginary part ϵ''_r , respectively. Each thin solid line designates a Maxwell-Wagner (MW) calculation³² fitted into each experimental result. The inset is the temperature dependence of $d\epsilon'_r/dT$.

tive anomaly, and two magnetic anomalies as follows, and plot them in Fig. 6 (a). (1) For the peak in the real part of the dielectric constant, the temperature at which $d\epsilon'_r/dT$ becomes zero is defined as the characteristic temperature $T_{\epsilon'-\text{peak}}$. The positions are shown by arrows in Fig. 5 (a). (2) For the sharp decrease in the real part of the dielectric constant, the temperature at which $d\epsilon'_r/dT(T)$ exhibits a sharp peak is defined as the characteristic temperature $T_{\epsilon'-\text{sd}}$, an example of which is shown in the inset of Fig. 3. (3) For the shoulder structure in the imaginary part of the dielectric constant, the kink tempera-

ture at which $d\epsilon''_r/dT(T)$ exhibits the minimum value is defined as the characteristic temperature $T_{\epsilon''-\text{sh}}$, an example of which is shown in the inset of Fig. 5 (b). (4) For the resistivity anomaly, the temperature T_ρ is determined from the small jump-like anomaly in the local activation energy $E_{\text{local}}(T) = d(\ln\rho)/d(1/T)$, as shown by an arrow in the inset of Fig. 2(b). (5 and 6) For the kink and remarkable increase in magnetization, which are shown by arrows in Fig. 2 (d), the characteristic temperatures $T_{M-\text{kink}}$ and $T_{M-\text{inc}}$ are determined from $dM/dT(T)$. For $x = 0.1$ and 0.3 , another kink

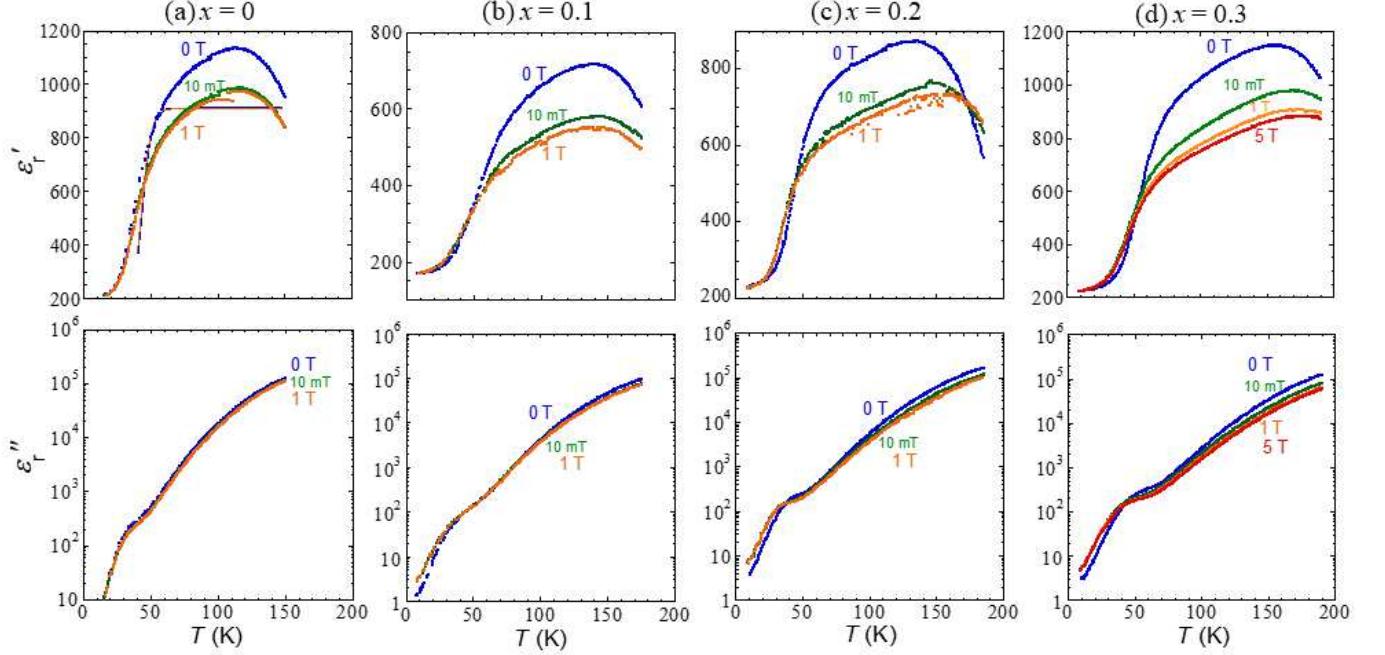


FIG. 4. Temperature dependence of the relative dielectric constant of polycrystalline $\text{Ca}_{1-x}\text{Sr}_x\text{Mn}_{0.85}\text{Sb}_{0.15}\text{O}_3$ under several magnetic fields after field cooling. (AC electric field of 1 V/mm and 10 kHz) (a) $x = 0$, (b) $x = 0.1$, (c) $x = 0.2$, and (d) $x = 0.3$. In the upper panel of (a), two thin solid lines designate the MW calculation³² fitted into the result for 0 T and 1 T. Because the resistivity of $\text{Ca}_{1-x}\text{Sr}_x\text{Mn}_{0.85}\text{Sb}_{0.15}\text{O}_3$ rarely exhibits magnetic-field dependence, the two MW curves of 0 T and 1 T almost overlap.

is observed at approximately 70 K and 90 K, respectively. Concerning these additional kinks, we hope to obtain detailed information via specific heat measurements in future work. To summarize the tendency of the anomaly temperatures, we clarified that $T_{\epsilon' - \text{peak}}$, T_ρ , and $T_{M - \text{kink}}$ exhibit a similar value and are enhanced together by Sr substitution, as shown in Fig. 6 (a). Moreover, $T_{\epsilon' - \text{sd}}$ corresponds well to $T_{\epsilon'' - \text{sh}}$. They remain at almost the same value under isovalent Sr substitution.

IV. DISCUSSION

From the broad large-value dielectric peak that exhibits a frequency dependence, $\text{Ca}_{1-x}\text{Sr}_x\text{Mn}_{0.85}\text{Sb}_{0.15}\text{O}_3$ seems to be a dielectric glass. However, we should carefully examine whether the observed dielectric characters are intrinsic. A large value of ϵ'_r can also be caused by the MW effect at interfaces like grain boundaries^{34–36}. In the MW model, the apparent relative dielectric constant ϵ'_{cal} is

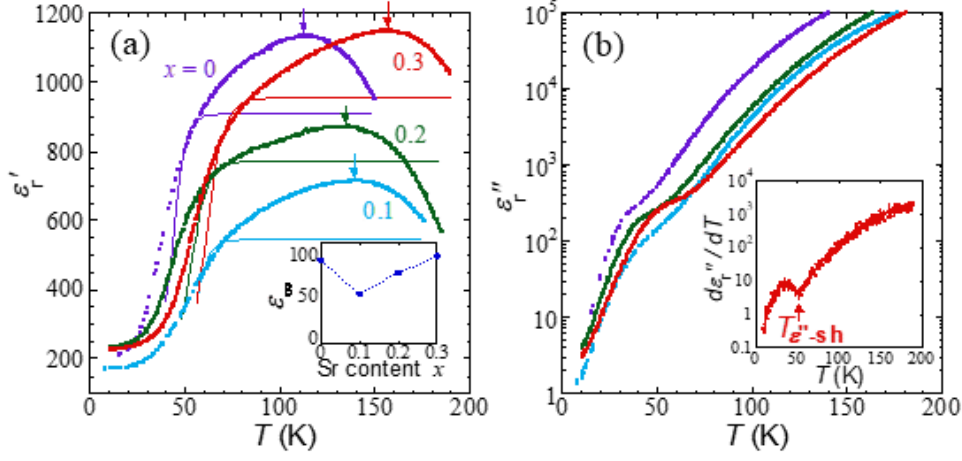


FIG. 5. Comparison of the relative dielectric constant among $\text{Ca}_{1-x}\text{Sr}_x\text{Mn}_{0.85}\text{Sb}_{0.15}\text{O}_3$ ($x = 0, 0.1, 0.2$ and 0.3) under a magnetic field of 0 T and an AC electric field of 1 V/mm and 10 kHz after field cooling. In panel (a), arrows indicate the peak position and thin solid lines designate the MW calculation³². The inset of (a) is the Sr content dependence of ϵ_∞ which is a parameter of MW fitting. The inset of (b) is the temperature dependence of $d\epsilon''/dT$ for $x = 0.3$. The arrow indicates the minimum temperature, which is defined as the shoulder temperature $T_{\epsilon''\text{-sh}}$.

described as follows³²:

$$\epsilon'_{\text{cal}}(T) = \frac{1}{C_0(R_1 + R_2)} \frac{\tau_1 + \tau_2 - \tau + \omega^2 \tau_1 \tau_2 \tau}{1 + \omega^2 \tau^2} \quad (1)$$

$$\epsilon''_{\text{cal}} = \frac{1}{\omega C_0(R_1 + R_2)} \frac{1 - \omega^2 \tau_1 \tau_2 + \omega^2 \tau(\tau_1 + \tau_2)}{1 + \omega^2 \tau^2} \quad (2)$$

Here, $C_0 = \epsilon_0 S/t$, ϵ_0 : electric constant, S : sample area, and t : sample thickness. C_i and R_i : capacitance and resistance of the corresponding phase, respectively, index $i = 1$ and 2 : grain-boundary layers and semiconducting grains, respectively. $\tau_1 = C_1 R_1$, $\tau_2 = C_2 R_2$, $\tau = (\tau_1 R_2 + \tau_2 R_1)/(R_1 + R_2)$. ω : angular frequencies. Notably, the values of ϵ'_T and ϵ''_T in this formula are determined by the ratio of the thickness, area, resistivity, and permittivity between the

two phases. According to Catalan's assumption³², in which $t_1/t_2 = 0.1$, $S_1 = S_2$, $\rho_1/\rho_2 = 100$, and $\epsilon_1 = \epsilon_2$ (t_i , S_i , ρ_i and ϵ_i : thickness, area, resistivity and intrinsic permittivity of the corresponding phase, respectively), Eq. (1), Eq. (2), and the relaxation time τ are transformed as follows:

$$\epsilon'_{\text{cal}}(T) = \frac{\epsilon_\infty}{10} \frac{91 + 1000(\epsilon_0 \epsilon_\infty \omega \cdot \rho_2(T))^2}{1 + 100(\epsilon_0 \epsilon_\infty \omega \cdot \rho_2(T))^2} \quad (3)$$

$$\epsilon''_{\text{cal}} = \frac{1}{10\omega\epsilon_0\rho} \frac{1 + 910(\epsilon_0 \epsilon_\infty \rho \omega)^2}{1 + 100(\epsilon_0 \epsilon_\infty \rho \omega)^2} \quad (4)$$

$$\tau(T) = 10\epsilon_0 \epsilon_\infty \cdot \rho_2(T) \quad (5)$$

Here, $\epsilon_\infty \equiv \epsilon_2/\epsilon_0$. For fitting Eq. (3) and Eq. (4) into the observed ϵ'_T and ϵ''_T , we adopted the observed DC resistivity values as ρ_2 of semiconducting grains because the conducting paths

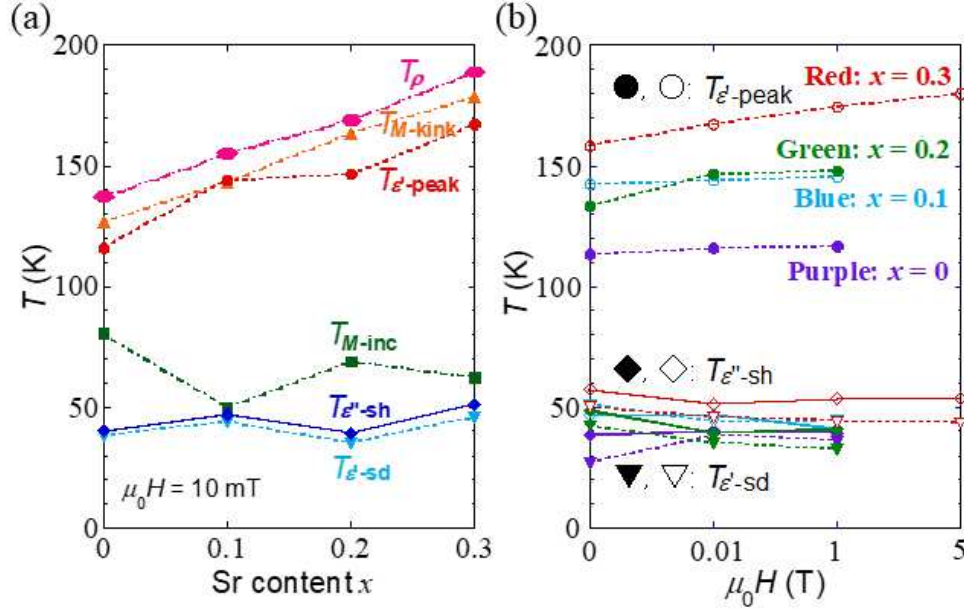


FIG. 6. (a) Sr-content and (b) magnetic-field dependence of the anomaly temperatures in the dielectric constant, resistivity, and magnetization of $\text{Ca}_{1-x}\text{Sr}_x\text{Mn}_{0.85}\text{Sb}_{0.15}\text{O}_3$ ($x = 0, 0.1, 0.2$ and 0.3). Hexagons, triangles, circles, rectangles, diamonds, and reversed triangles indicate T_ρ , $T_{M\text{-kink}}$, $T_{E'\text{-peak}}$, $T_{M\text{-inc}}$, $T_{E''\text{-sh}}$ and $T_{E'\text{-sd}}$, respectively. These anomaly temperatures are defined later in the text.

of the majority phase 2 with higher electric conductivity determine the observed resistivity values in the case of the larger volume fraction $t_1/t_2 = 0.1$. As shown in Fig. 3, although the sharp decrease of ϵ'_t and the shoulder structure of ϵ''_t are reproduced by the MW model, the peak of ϵ'_t is not. Therefore, the peak structure of ϵ'_t is expected to be intrinsic. Moreover, the calculation ϵ'_{cal} does not exhibit a frequency dependence at high temperatures, including $T_{E'\text{-peak}}$. This result suggests that the frequency dependence of ϵ'_t near $T_{E'\text{-peak}}$ is also intrinsic. The value of the fitting parameter ϵ_∞ , which is plotted in the inset

of Fig. 5(a), is consistent with that of a similar system $\text{La}_{1-x}\text{Ca}_x\text{MnO}_3$ (about 20-100)⁶.

In the low and high temperature limits for the MW model, we obtained $\epsilon'_{\text{cal}}(\text{Low-}T) = \epsilon_\infty$ and $\epsilon'_{\text{cal}}(\text{high-}T) = 9.1 \epsilon_\infty$. At high temperatures, the apparent dielectric constant was enhanced by the reduced effective thickness because of the good conducting grains surrounded by the insulating grain boundaries. $\epsilon'_{\text{cal}}(\text{Low-}T)$ and $\epsilon'_{\text{cal}}(\text{high-}T)$ were responsible for the high and low frequency limits, $\omega\tau \gg 1$ and $\omega\tau \ll 1$, respectively. Table II shows that the characteristic temperatures T_0 estimated from the expression of the MW-model-based relaxation agree well

TABLE II. Characteristic values in the dielectric properties of $\text{Ca}_{1-x}\text{Sr}_x\text{Mn}_{0.85}\text{Sb}_{0.15}\text{O}_3$ ($x = 0, 0.1, 0.2$, and 0.3). Former four values $T_{\varepsilon'-\text{peak}}$, $\varepsilon'_{\text{obs}}(T=T_{\varepsilon'-\text{peak}})$, $\frac{\varepsilon'_{\text{obs}}(1\text{ T})-\varepsilon'_{\text{obs}}(0\text{ T})}{\varepsilon'_{\text{obs}}(0\text{ T})}$ ($T=T_{\varepsilon'-\text{peak}}$), and $T_{\varepsilon''-\text{sh}}$ are estimated from measurement at 10 kHz. The latter three values $\varepsilon'_{\text{cal}}(\text{low-}T)$, $\varepsilon'_{\text{cal}}(\text{high-}T)$, and T_0 are obtained from the calculation based on the MW model³².

x	$T_{\varepsilon'-\text{peak}}$ (K)	$\varepsilon'_{\text{obs}}(T=T_{\varepsilon'-\text{peak}})$	$\frac{\varepsilon'_{\text{obs}}(1\text{ T})-\varepsilon'_{\text{obs}}(0\text{ T})}{\varepsilon'_{\text{obs}}(0\text{ T})}$ ($T=T_{\varepsilon'-\text{peak}}$) (%)	$T_{\varepsilon''-\text{sh}}$ (K)	$\varepsilon'_{\text{cal}}(\text{low-}T)$	$\varepsilon'_{\text{cal}}(\text{high-}T)$	T_0 (K)
0.0	113	1136	-14.4	38	100	910	43
0.1	142	717	-23.0	47	60	546	56
0.2	133	875	-17.1	49	85	774	52
0.3	158	1151	-22.3	58	105	956	61

with the shoulder temperatures $T_{\varepsilon''-\text{sh}}$ for all the measured samples. Here, T_0 is the characteristic temperature of the dielectric loss at which $\omega\tau = 1$. For 10 kHz, we obtained the value of $\rho_2(T_0)$ from Eq. (5) and estimated the corresponding temperature T_0 from the $\rho(T)$ data in Fig. 2 (a).

In Fig. 7, we show the Arrhenius plots from the dielectric-loss shoulder temperature $T_{\varepsilon''-\text{sh}}$ and the dielectric peak temperature $T_{\varepsilon'-\text{peak}}$ measured at three frequencies ($f = 10, 50$, and 100 kHz). In Table III, the activation energy E_a and relaxation time τ_0 from the Arrhenius plots using $1/2\pi f = \tau = \tau_0 \exp(E_a/k_B T)$ are listed as a function of Sr content. The parameters, E_{a1} and τ_{01} , are related to the relaxation process of the heterogeneous material consisting of grain-boundaries and semiconducting grains. In contrast, E_{a2} and τ_{02} estimated from

the dielectric peak temperature $T_{\varepsilon'-\text{peak}}$ are associated with the relaxation process of localized charges. In particular, E_{a2} and τ_{02} are comparable to the typical values of polaronic relaxation in CaMnO_3 and other perovskites⁷. The values of E_{a2} estimated from the dielectric peak are also not very different from the small polaron hopping energies $E_{a,\rho}$ estimated from the resistivity data. Therefore, we suggest that the high-temperature dielectric and transport data strongly indicate the polaronic nature of the present system.

In addition to the above calculations, we also measured the dielectric constant of a single-crystalline $\text{CaMn}_{0.88}\text{Sb}_{0.12}\text{O}_3$ (thickness: 0.75 mm, cross-sectional area: 13.0 mm^2) to verify the influence of the MW effect³⁶, as shown in Fig. 8. The MW effect originating from grain boundaries can be excluded in

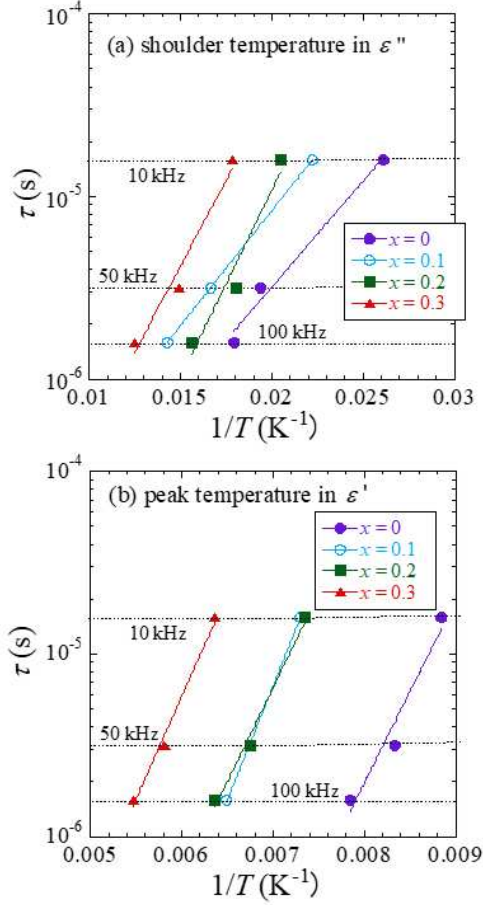


FIG. 7. Arrhenius plots from (a) the dielectric-loss shoulder temperature $T_{\varepsilon''-\text{sh}}$ and (b) the dielectric peak temperature $T_{\varepsilon'-\text{peak}}$ measured at three frequencies ($f = 10, 50$, and 100 kHz).

single-crystalline samples. In the single crystal, $\varepsilon'_r(T)$ exhibits a broad peak at a temperature that is consistent with $T_{\varepsilon'-\text{peak}}$ of the polycrystal with the same chemical composition, as shown in the inset of Fig 8. This reproducibility of $T_{\varepsilon'-\text{peak}}$ indicates that the large-value broad peak of $\varepsilon'_r(T)$ in $\text{Ca}_{1-x}\text{Sr}_x\text{Mn}_{0.85}\text{Sb}_{0.15}\text{O}_3$ is not the MW effect but an intrinsic phenomenon. In contrast, the sharp decrease of ε'_r and the

TABLE III. Activation energy E_a and relaxation time τ_0 obtained from the Arrhenius plots using $1/2\pi f = \tau = \tau_0 \exp(E_a/k_B T)$, with E_{a1} and τ_{01} being determined from the frequency dependence of the dielectric-loss shoulder temperature $T_{\varepsilon''-\text{sh}}$. E_{a2} and τ_{02} were estimated from the dielectric peak temperature $T_{\varepsilon'-\text{peak}}$.

x	E_{a1} (meV)	τ_{01} (s)	E_{a2} (meV)	τ_{02} (s)
0.0	23	1.5×10^{-8}	198	2.1×10^{-14}
0.1	25	2.5×10^{-8}	248	1.2×10^{-14}
0.2	41	8.4×10^{-10}	204	4.0×10^{-13}
0.3	37	6.2×10^{-9}	264	3.0×10^{-14}

shoulder of ε''_r were not observed in the single-crystalline sample, suggesting that these two anomalies at approximately 45 K are caused by the MW effect.

Regarding the magnetic-field dependence of ε'_r , we should note that an apparent effect can be caused by the combination of magnetoresistance and MW effect^{32,38}. In addition, from this viewpoint, we can exclude the possibility that the dielectric peak is caused by the MW effect. When the combination of magnetoresistance and MW effect causes the apparent "magneto-capacitance effect", the sign of the "magneto-capacitance effect" changes depending on whether the magnetoresistance occurs at the sample core or at the interface³². First, for the core-dominated magne-

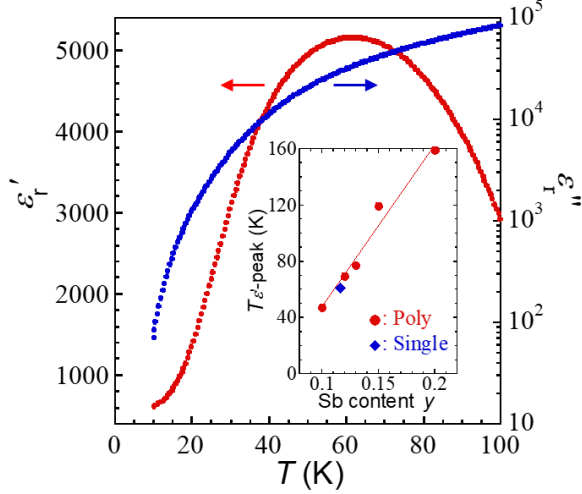


FIG. 8. Temperature dependence of the relative dielectric constant of single-crystalline $\text{CaMn}_{0.88}\text{Sb}_{0.12}\text{O}_3$ under 0 T. (AC electric field of 1 V/mm and 10 kHz) Inset represents $T_{\epsilon'-\text{peak}}$ s of $\text{CaMn}_{1-y}\text{Sb}_y\text{O}_3$. $T_{\epsilon'-\text{peak}}$ of the single crystal designated by the diamond agreed well with the curve fitted into $T_{\epsilon'-\text{peak}}$ s of polycrystals designated by circles³⁷.

toresistance, which is detectable in the high-frequency conductivity, the sign of "magneto-capacitance effect" is positive. In contrast, the sign of the observed magneto-capacitance effect is negative in $\text{Ca}_{1-x}\text{Sr}_x\text{Mn}_{0.85}\text{Sb}_{0.15}\text{O}_3$. Thus, the origin of the magneto-capacitance effect in $\text{Ca}_{1-x}\text{Sr}_x\text{Mn}_{0.85}\text{Sb}_{0.15}\text{O}_3$ is not core-dominated magnetoresistance. Second, for the interface-dominated magnetoresistance, which is detectable in the low-frequency conductivity, the magnetoresistance of $\text{CaMn}_{0.85}\text{Sb}_{0.15}\text{O}_3$ seems to be within the error margin, as shown in

Fig. 2 (c). Using the measured resistivity value, we calculated the dielectric constant of the MW effect for 0 T and 1 T based on Eq. (3). As shown in Fig. 4(a), the two calculation curves almost overlapped and could not explain the observed significant magnetic-field effect. Thus, the origin of the magneto-capacitance effect in $\text{Ca}_{1-x}\text{Sr}_x\text{Mn}_{0.85}\text{Sb}_{0.15}\text{O}_3$ was not interface-dominated magnetoresistance. Therefore, we conclude that the magneto-capacitance effect in $\text{Ca}_{1-x}\text{Sr}_x\text{Mn}_{0.85}\text{Sb}_{0.15}\text{O}_3$ which is significant at $T_{\epsilon'-\text{peak}}$ is an intrinsic phenomenon.

From the above discussion, the dielectric characters that are expected to be intrinsic are (1) the broad peak structure of $\epsilon'_r(T)$, (2) the frequency dependence of this peak, and (3) the negative magnetic-field effect on this peak. Because the Arrhenius plots identified the dielectric peak as a phenomenon originating from polarons, the peak suggests that below the peak temperature $T_{\epsilon'-\text{peak}}$, it becomes difficult for dipole moments consisting of polarons to change their direction following the plus-minus switching of an applied AC electric field. This behavior can be attributed to the spontaneous dipole ordering; the relaxation time and the activation energy suggest that polarons form the dipole ordering. In the charge-ordering system $\text{Pr}_{1-x}\text{Ca}_x\text{MnO}_3$ whose broad dielectric peak and high conductivity are similar to those of $\text{Ca}_{1-x}\text{Sr}_x\text{Mn}_{0.85}\text{Sb}_{0.15}\text{O}_3$ ^{8,9,11}, the electric polarization is directly proved

by the positive-up-negative-down method³³. Thus, by analogy with $\text{Pr}_{1-x}\text{Ca}_x\text{MnO}_3$, it is reasonable to expect electric polarization in $\text{Ca}_{1-x}\text{Sr}_x\text{Mn}_{0.85}\text{Sb}_{0.15}\text{O}_3$ below $T_{\epsilon' - \text{peak}}$, at least microscopically.

A broad frequency-dependent peak is commonly observed in dielectric glasses³⁹. Moreover, the ion arrangement of $\text{Ca}_{1-x}\text{Sr}_x\text{Mn}_{0.85}\text{Sb}_{0.15}\text{O}_3$ in which different ions exist on crystallographically equivalent sites is favorable for some dielectric glasses. Therefore, we speculate that $\text{Ca}_{1-x}\text{Sr}_x\text{Mn}_{0.85}\text{Sb}_{0.15}\text{O}_3$ is a dielectric glass consisting of clusters with a short-range dipole ordering: Because the substituted Sb ions induce disorder (inhomogeneity) into the Mn sites and curb the Mn-Mn interaction, the dipole ordering caused by an Mn-Mn interaction is of the short-range in $\text{Ca}_{1-x}\text{Sr}_x\text{Mn}_{0.85}\text{Sb}_{0.15}\text{O}_3$. As a similar example, a spin-glass state is observed in $\text{CaMn}_{1-y}\text{Sb}_y\text{O}_3$ ($0.02 \leq y \leq 0.05$)¹⁴.

With respect to coupling between the dielectric and conducting properties, the similarities in values and the positive correlation in the Sr substitution between $T_{\epsilon' - \text{peak}}$ and T_ρ suggest that the dielectric peak is related to CO in $\text{Ca}_{1-x}\text{Sr}_x\text{Mn}_{0.85}\text{Sb}_{0.15}\text{O}_3$ ($x = 0, 0.1, 0.2$, and 0.3). It is expected that the peak of $\epsilon'_t(T)$ is not a secondary anomaly which accompanies changes in conductivity, but it is an intrinsic anomaly originating from capacitive charges. If a dielectric anomaly is dominated by con-

ductivity, ϵ''_t which contains the effect of conductivity as well as the dielectric loss will exhibit a more drastic anomaly than ϵ'_t . However, ϵ''_t of $\text{Ca}_{1-x}\text{Sr}_x\text{Mn}_{0.85}\text{Sb}_{0.15}\text{O}_3$ does not exhibit an anomaly at $T_{\epsilon' - \text{peak}}$; an example is shown in the inset of Fig. 5 (b). Even the temperature derivative that can detect a subtle anomaly does not change at $T_{\epsilon' - \text{peak}}$. Therefore, we consider that the dielectric peak in $\text{Ca}_{1-x}\text{Sr}_x\text{Mn}_{0.85}\text{Sb}_{0.15}\text{O}_3$ is caused by the ordering of localized polarons. CO is a possible example of this ordering.

The magneto-capacitance effect in $\text{Ca}_{1-x}\text{Sr}_x\text{Mn}_{0.85}\text{Sb}_{0.15}\text{O}_3$ can be understood by the hypothesis that a spontaneous dipole ordering along a certain direction is stabilized by a magnetic field. The suppression of the peak height of ϵ'_t by a magnetic field suggests that the magnetic field fixes the direction of dipole moments in $\text{Ca}_{1-x}\text{Sr}_x\text{Mn}_{0.85}\text{Sb}_{0.15}\text{O}_3$ and disturbs their response to an applied AC electric field. The enhancement of $T_{\epsilon' - \text{peak}}$ for $x \geq 0.2$ shown in Fig. 6 (b) indicates that the magnetic field supports a dipole ordering.

The stabilization of the spontaneous dipole ordering along a certain direction by a magnetic field can be explained by the character of $\text{Ca}_{1-x}\text{Sr}_x\text{Mn}_{0.85}\text{Sb}_{0.15}\text{O}_3$, i.e., the dipole ordering seems to accompany an AFM ordering. Under 0 T, in a system that has multi crystallographically equivalent axes, a magnetic/dipole ordering possesses several possible directions

that are degenerated. A magnetic field introduces anisotropy into the system and fixes the direction of the magnetic ordering. Because a one-to-one correspondence is expected between the direction of the dipole ordering and that of the AFM ordering, the direction of the dipole ordering is also fixed by a magnetic field.

Next, we discuss why the substitution of Sr in this compound remarkably increases $T_{\epsilon' - \text{peak}}$, T_p and $T_{M - \text{kink}}$ by more than 40 K from $x = 0$ to 0.3. Because the Sr^{2+} ion is isovalent to the Ca^{2+} ion, the change of the electronic properties is expected to be caused by a lattice deformation. As shown in Table I, the tolerance factor $t = \frac{r_A + r_O}{\sqrt{2}(r_B + r_O)}$ changes from 0.9896 at $x = 0$ to 1.000 at $x = 0.3$. (r_A , r_B , and r_O are ionic radii of A, B, and O ion in the ABO_3 perovskite, respectively.) The change of t suggests that Mn-O-Mn angles approach 180° . Therefore, we consider that Sr substitution enhances the AFM superexchange interaction between Mn^{4+} ions and assists in the formation of an AFM ordering that is accompanied by a dipole ordering.

As the next issue, it would be important to clarify whether macroscopic electric polarization exists at low temperatures. Because $\text{Ca}_{1-x}\text{Sr}_x\text{Mn}_{0.85}\text{Sb}_{0.15}\text{O}_3$ exhibits relatively high conductivity, the positive-up-negative-down method would be required^{33,40–43}. It would also be interesting to investigate the anisotropy of the dielectric properties using single crystals.

V. SUMMARY

We measured the dielectric constant, resistivity, and magnetization of electron-doped manganite $\text{Ca}_{1-x}\text{Sr}_x\text{Mn}_{0.85}\text{Sb}_{0.15}\text{O}_3$ ($x = 0, 0.1, 0.2$, and 0.3). The temperature dependence of the dielectric constant shows a broad and large peak above 110 K in the real part, followed by a sharp decrease at approximately 45 K, at which the imaginary part exhibits a shoulder structure. The sharp decrease in ϵ'_f and the shoulder structure in ϵ''_f can be understood by the MW scenario. The apparent colossal dielectric constant is partially explained by the reduced effective thickness due to the good conducting grains surrounded by the insulating grain boundaries at high temperatures. However, for the following three reasons, the peak in ϵ'_f is expected to be intrinsic and suggests a dipole ordering of polarons: (1) the peak cannot be reproduced by calculations based on the MW model; (2) the values of the relaxation time and the activation energy that are estimated from the frequency dependence of the peak temperature are typical of polaronic relaxation; and (3) the peak is observed similarly in single-crystalline samples. The peak height is suppressed and the peak temperature is enhanced by increasing frequency. This frequency dependence suggests that $\text{Ca}_{1-x}\text{Sr}_x\text{Mn}_{0.85}\text{Sb}_{0.15}\text{O}_3$ is a dielectric glass. This hypothesis is reasonable because Sb substitution introduces inho-

mogeneity in the Mn lattice, and dielectric glasses are often found in such inhomogeneous systems. Because the temperature of the dielectric peak is similar to that of the resistivity anomaly which suggests a CO, the dipole ordering in $\text{Ca}_{1-x}\text{Sr}_x\text{Mn}_{0.85}\text{Sb}_{0.15}\text{O}_3$ might be driven by CO. This dipole ordering accompanies AFM ordering because a magnetization kink was observed near the peak temperature of $\epsilon'_r(T)$. Notably, we revealed that the dielectric peak exhibits a negative magnetic-field effect, which cannot be explained by magnetoresistance. We consider that the AFM ordering in $\text{Ca}_{1-x}\text{Sr}_x\text{Mn}_{0.85}\text{Sb}_{0.15}\text{O}_3$ is the glue between the magnetic field and dipole ordering and causes the magneto-capacitance effect. Substituting Ca^{2+} with isovalent Sr^{2+} remarkably enhances the temperature of the dielectric peak by 50 K probably because Mn-O-Mn buckling is released and the AFM super-exchange interaction between Mn^{4+} ions is enhanced.

ACKNOWLEDGMENTS

We acknowledge Y. Ishii, H. Yamamoto, S. Sekikawa, and H. Kimura for fruitful discussions, T. Yajima for the technical support, and H. Fujishiro for the advice on scientific writing. This work is supported by Iwate University, JSPS KAKENHI Grant Number JP17K14101, and Visiting Researcher's Program of the ISSP. One of the authors (T. W.) was supported by Hi-

rosaki University Grant for Distinguished Researchers FY2017-2018. We would like to thank Editage (www.editage.com) for English language editing.

REFERENCES

- ¹Y. Tokura, H. Kuwahara, Y. Moritomo, Y. Tomioka, and A. Asamitsu, *Phys. Rev. Lett.* **76**, 3184 (1996).
- ²Z. Zeng, M. Greenblatt, and M. Croft, *Phys. Rev. B* **63**, 224410 (2001).
- ³A. Maignan, C. Martin, C. Autret, M. Hervieu, B. Raveau, and J. Hejtmanek, *J. Mater. Chem.* **12**, 1806 (2002).
- ⁴E. N. Caspi, M. Avdeev, S. Short, J. D. Jorgensen, M. V. Lobanov, Z. Zeng, M. Greenblatt, P. Thiyagarajan, C. E. Botez, and P. W. Stephens, *Phys. Rev. B* **69**, 104402 (2004).
- ⁵T. Okuda and Y. Fujii, *J. Appl. Phys.* **108**, 103702 (2010).
- ⁶J. L. Cohn, M. Peterca, and J. J. Neumeier, *Phys. Rev. B* **70**, 214433 (2004).
- ⁷J. L. Cohn, M. Peterca, and J. J. Neumeier, *J. Appl. Phys.* **97**, 034102 (2005).
- ⁸C. Jardón, F. Rivadulla, L. E. Hueso, A. Fondado, M. A. López-Quintela, J. Rivas, R. Zysler, M. T. Causa, and R. D. Sánchez, *J. Magn. Magn. Mater.* **196**, 475 (1999).
- ⁹S. Mercone, A. Wahl, A. Pautrat, M. Pollet, and C. Simon, *Phys. Rev. B* **69**, 174433 (2004).

- ¹⁰R. S. Freitas, J. F. Mitchell, and P. Schiffer, Phys. Rev. B **72**, 144429 (2005).
- ¹¹C. R. Serrao, A. Sundaresan, and C. N. R. Rao, J. Phys.: Condens. Matter **19**, 496217 (2007).
- ¹²J. R. Sahu, C. R. Serrao, A. Ghosh, A. Sundaresan, and C. N. R. Rao, Solid State Communications **149**, 49 (2009).
- ¹³Y. Murano, M. Matsukawa, S. Kobayashi, S. Nimori, and R. Suryanarayanan, J. Phys.: Conf. Ser. **200**, 012114 (2010).
- ¹⁴Y. Murano, M. Matsukawa, S. Ohuchi, S. Kobayashi, S. Nimori, R. Suryanarayanan, K. Koyama, and N. Kobayashi, Phys. Rev. B **83**, 054437 (2011).
- ¹⁵T. Fujiwara, M. Matsukawa, S. Ohuchi, S. Kobayashi, S. Nimori, and R. Suryanarayanan, J. Kor. Phys. Soc. **62**, 1925 (2013).
- ¹⁶T. Fujiwara, M. Matsukawa, T. Aoyagi, S. Kobayashi, H. Taniguchi, S. Nimori, and R. Suryanarayanan, J. Magn. Magn. Mater. **378**, 451 (2015).
- ¹⁷H. Taniguchi, H. Takahashi, A. Terui, S. Kobayashi, M. Matsukawa, and R. Suryanarayanan, J. Phys.: Conf. Ser. **969**, 012094 (2018).
- ¹⁸M. Fiebig, T. Lottermoser, D. Frohlich, A. V. Goltsev, and R. V. Pisarev, Nature **419**, 818 (2002).
- ¹⁹B. Lorenz, Y.-Q. Wang, and C.-W. Chu, Phys. Rev. B **76**, 104405 (2007).
- ²⁰H. Katsura, N. Nagaosa, and A. V. Balatsky, Phys. Rev. Lett. **95**, 057205 (2005).
- ²¹I. A. Sergienko and E. Dagotto, Phys. Rev. B **73**, 094434 (2006).
- ²²T. Arima, J. Phys. Soc. Jpn. **76**, 073702 (2007).
- ²³N. Ikeda, K. Kohn, N. Myouga, E. Takahashi, H. Kitoh, and S. Takekawa, J. Phys. Soc. Jpn. **69**, 1526 (2000).
- ²⁴D. V. Efremov, J. Brink, and D. I. Khomskii, Nature Materials **3**, 853 (2004).
- ²⁵D. V. Efremov, J. Brink, and D. I. Khomskii, Physica B **359**, 1433 (2005).
- ²⁶N. Ikeda, H. Ohsumi, K. Ohwada, K. Ishii, T. Inami, K. Kakurai, Y. Murakami, K. Yoshii, S. Mori, Y. Horibe, et al., Nature **436**, 1136 (2005).
- ²⁷D. I. Khomskii, J. Magn. Magn. Mater. **306**, 1 (2006).
- ²⁸A. Nagano, M. Naka, J. Nasu, and S. Ishihara, Phys. Rev. Lett. **99**, 217202 (2007).
- ²⁹J. Brink and D. I. Khomskii, J. Phys.: Condens. Matter **20**, 434217 (2008).
- ³⁰G. Giovannetti, S. Kumar, J. van den Brink, and S. Picozzi, Phys. Rev. Lett. **103**, 037601 (2009).
- ³¹V. Poltavets, K. Vidyasagar, and M. Jansen, Solid State Chem. **177**, 1285 (2004).
- ³²G. Catalan, Appl. Phys. Lett. **88**, 102902 (2006).
- ³³V. K. Shukla, S. Mukhopadhyay, K. Das, A. Sarma, and I. Das, Phys. Rev. B **90**, 245126 (2014).

- (2014).
- ³⁴A. R. von Hippel, *Dielectrics and Waves* (Wiley, London, 1954).
- ³⁵P. Lunkenheimer, V. Bobnar, A. V. Pronin, A. I. Ritus, A. A. Volkov, and A. Loidl, Phys. Rev. B **66**, 052105 (2002).
- ³⁶P. Lunkenheimer, S. Krohns, S. Riegg, S. G. Ebbinghaus, A. Reller, and A. Loidl, Eur. Phys. J. Special Topics **180**, 61 (2010).
- ³⁷H. Taniguchi, H. Takahashi, A. Terui, S. Kobayashi, M. Matsukawa, and R. Suryanarayanan, IEEE Trans. Magn. **55**, 1000104 (2019).
- ³⁸S. Kamba, D. Nuzhnyy, M. Savinov, J. Šebek, J. Petzelt, J. Prokleška, R. Haumont, and J. Kreisel, Phys. Rev. B **75**, 024403 (2007).
- ³⁹A. A. Bokov and Z.-G. Ye, J. Mater. Sci. **41**, 31 (2006).
- ⁴⁰S. D. Traynor, T. D. Hadnagy, and L. Kammerdiner, Integr. Ferroelectrics **16**, 63 (1997).
- ⁴¹S. Y. Yang, F. Zavaliche, L. Mohaddes-Ardabili, V. Vaithyanathan, D. G. Schlom, Y. J. Lee, Y. H. Chu, M. P. Cruz, Q. Zhan, T. Zhao, et al., Appl. Phys. Lett. **87**, 102903 (2005).
- ⁴²M. Fukunaga and Y. Noda, J. Phys. Soc. Jpn. **77**, 064706 (2008).
- ⁴³H. Naganuma, Y. Inoue, and S. Okamura, Appl. Phys. Express **1**, 061601 (2008).